Computational and Structural Biotechnology Journal 21 (2023) 742–750

Contents lists available at ScienceDirect

Computational and Structural Biotechnology Journal

journal homepage: www.elsevier.com/locate/csbj

Cell segmentation and representation with shape priors

Dominik Hirling [a,b], Peter Horvath [a,c,d,*]

[a] Synthetic and Systems Biology Unit, Biological Research Centre (BRC), Hungary
[b] Doctoral School of Computer Science, University of Szeged, Hungary
[c] Institute for Molecular Medicine Finland, University of Helsinki, Finland
[d] Single-Cell Technologies Ltd, Hungary

ARTICLE INFO

Article history:
Received 12 August 2022
Received in revised form 18 December 2022
Accepted 19 December 2022
Available online 29 December 2022

Keywords:
Shape representation
Deep learning
Fourier descriptors
Statistical shape models
Cell segmentation

ABSTRACT

Cell segmentation is a fundamental problem of computational biology, for which convolutional neural networks yield the best results nowadays. This field is expanding rapidly, and in the recent years, shape-constrained segmentation models emerged as strong competitors to traditional, pixel-based segmentation methods for instance segmentation. These methods predict the parameters of the underlying shape model, so choosing the right shape representation is critical for the success of the segmentation. In this study, we introduce two new representation-based deep learning segmentation methods after a quantitative comparison of the most important shape descriptors in the literature. Our networks are based on Fourier coefficients and statistical shape models, both of which have proven to be reliable tools for cell shape modelling. Our results indicate that the methods are competitive alternatives to the most widely used baseline deep learning algorithms, especially when the number of parameters for the underlying shape model are low or the cells to be segmented have irregular morphologies.

1. Introduction

Imaging, identifying, and morpho-measuring cells and their subcellular compartments are often the first step of fundamental cell biology research and drug discovery. Single cell segmentation is an important part of this, as it enables researchers to analyze the number of cells, their shapes, phenotypes or physiological state on microscopic images. In the recent years, convolutional neural networks emerged as an effective tool for tackling segmentation tasks [6], among them, U-Net [23] and Mask-R-CNN [8] can be considered the most widely used ones. U-Net is a dense pixel classifier network, with an encoder-decoder structure originally used for semantic segmentation, however, it can be modified to perform instance segmentation as well and is still used in many biomedical applications [11,17,21]. Mask R-CNN performs instance segmentation in two steps: first, the bounding boxes are regressed, after which the binary masks are produced inside the detected box. Mask R-CNN is still widely used, however, it requires a lot of hyperparameter tuning and training is also relatively slow [3]. The encoder-decoder structure is built up from ResNet (encoder) [9] and Feature pyramid network (FPN, decoder) [15]. Recently, a new generation of segmentation methods emerged that instead of per-pixel classification or bounding boxes, predict the parameters of an underlying cell model. This approach can be beneficial, because 1) instead of semantic segmentation, instance segmentation can be carried out much easier compared to the pixel-wise approach, 2) regressing shape descriptors can give extra information about the segmentation depending on what descriptors are used and 3) learning shape representations can be thought of as a regularization technique as well [13]. The most popular representations are star-convex polygons [24] and cubic B-splines [18] in 2D, and star-convex polyhedra [27] and spherical harmonics [5] in 3D. Choosing the right cell representation is crucial to the success of these methods, as certain shape descriptors may perform better or worse on particular datatypes or in general. There have been several studies about cell shape analysis unrelated to this application [22,28], but no quantitative comparison between a large number of representations for cell shape description has been carried out yet to our knowledge. In this study, our aim is to 1) extend the knowledge about shape-constrained cell segmentation and the possible uses of other representations and 2) provide information about which shape descriptors are the most appropriate for biological data. In this paper, we compare and quantitatively evaluate a large pool of possible cell shape models on real and synthetic images. We also

* Corresponding author at: Synthetic and Systems Biology Unit, Biological Research Centre (BRC), Hungary.

https://doi.org/10.1016/j.csbj.2022.12.034

introduce new cell representations with Fourier descriptors and statistical shape models, with two deep learning segmentation networks, similar in nature to the currently available StarDist [24] and SplineDist [18] architectures, but relying on the proposed cell representations. The source code can be found at https://bitbucket.org/biomag/cellrepresentation.

2. Related work

2.1. Cell representation techniques

Modelling shapes with a small number of parameters has been studied for a long time [29]. One of the most well known tools for describing objects (when looking at them as parametric curves) are orthogonal functions, which are essential in approximation theory, as they can be effectively used to describe functions with infinite series.

Definition 1. Functions g and h are orthogonal on interval $[a, b]$ with respect to a weight function w, if.

$$\langle g, h\rangle = \int_a^b w(x)g(x)h(x)dx = 0.$$

Let $\varphi_0, \varphi_1, \varphi_2, \ldots$ be a system of orthogonal functions on interval $[a, b]$, and let $c_0, c_1, c_2, \ldots$ be constants. The *generalized Fourier series*

$$f(x) = \sum_{n=0}^{\infty} c_n\varphi_n$$

represents f as a convergent series, where the coefficients c_n can be calculated from

$$c_n = \frac{\langle f, \varphi_n\rangle}{\langle \varphi_n, \varphi_n\rangle}.$$

The most well known set of orthogonal functions for describing shapes are trigonometric functions, which can be used for calculating the Fourier series expansion of a contour. Besides that, polynomial basis functions (e.g. Legendre, Hermite, Chebyshev polynomials) and wavelet functions (e.g. Haar wavelets) can be utilized as well. Using these functions can be beneficial due to the simple and explicit computation of the coefficients of the basis functions in the series, however, one does not necessarily need the orthogonality property to accurately describe contours, for example, B-splines have been successful in this area as well [18]. A spline contour of order n is a piecewise polynomial function with a degree of $n-1$. B-splines of a given order can be thought of as basis functions in the space of spline functions, which means that any piecewise polynomial function with a degree of $n-1$ can be described by a linear combination of B-splines of order n. The "weights" of the B-splines are the control points, which describe the curve implicitly. Usually, cubic B-splines are used ($n = 4$), and a contour is described by a function

$$\mathbf{s}(t) = \begin{bmatrix} x(t) \\ y(t) \end{bmatrix} = \sum_{k=0}^{M-1} \mathbf{c}[k]\varphi_M(t-k), \tag{1}$$

where M is the number of control points used, $\mathbf{c}$ is the vector of control points, and $\varphi_M(t) = \beta_M^3(t)$ are the cubic basis functions for M number of control points.

Another possibility is to use statistical shape models (SSM-s) [4], where an object is represented by k landmark points. Given a set of n shapes, after performing a step of procrustes analysis [7], one can perform principal component analysis on the matrix of shapes. The eigenvectors corresponding to the highest eigenvalues will represent the most important shape variations from the mean shape in the training set. Using a few of these extracted eigenvectors along with a rotation, translation, and a uniform scaling parameter, we can approximate any shape with the aforementioned parameters (assuming that the shape to be approximated is similar to the shapes in the training set, on which the PCA was performed). Specifically for cell description, the star-convex polygon representation became widespread with the introduction of the StarDist segmentation method, however, it only guarantees convergence for star-shaped objects Fig. 1.

2.2. Cell segmentation with geometric priors

The most well known segmentation methods nowadays are based on per-pixel classification, among them, Mask-RCNN [8] and U-Net [23] are used most of the time as baselines. Recently, a lot of research has been focused on incorporating structural information into neural networks about the objects that have to be segmented. This can be achieved by either modifying the loss function, predicting a parametric model instead of classifying each pixel or the combination of the two. In [13,20], authors have proposed a method where a shape encoder was incorporated into the neural network and the segmentations were based on the learned shape representations. Other solutions are related to the classical roots of segmentation, predicting the parameters of active contour models [19]. Specifically for biomedical image segmentation, one of the most successful method was StarDist [24], which regresses the radial distances of the cell contour, followed by SplineDist [18], which achieves accurate segmentation by using an underlying B-Spline model. These shape-constrained methods, with addition to the common benefits of shape parameter models, also have the advantage that they require a lot less hyper-parameter tuning and less network parameters in general compared to Mask-RCNN [24]. The Contour Proposal Network (CPN) is a very recent addition to the selection of segmentation methods utilizing shape prior information [26]. This network regresses Fourier coefficients, which are very natural and intuitive tools for cell shape description, as the most simplistic shape they can describe is an ellipsoid. One drawback of this method is that besides predicting the Fourier coefficients for the cell shape, the network also has a so-called refinement head, which further modifies the segmentation, making it hard to evaluate the descriptive capabilities of the coefficients themselves.

3. Methods

3.1. Cell representation

With this study, our aim is to find the most suitable cell representations, so that we can incorporate them into convolutional neural networks for accurate segmentation results. For that, we tested 8 different cell representations to select the most expressive ones for segmentations. All of the representations are used to approximate parametric, two-dimensional (2D) contours, so for evaluating these techniques, we first convert the binary masks into discretized curves, and then approximate these with 1) Orthogonal polynomials (Chebyshev, Legendre, Hermite), 2) Wavelet series (Haar), 3) Star-convex polygon representation, 4) Cubic B-Splines, 5) Fourier series and 6) Statistical shape models. After the approximation, we convert back the approximated contours into binary masks. Based on the results presented in Subsection 4.3, the most efficient descriptors for the types of images included in our

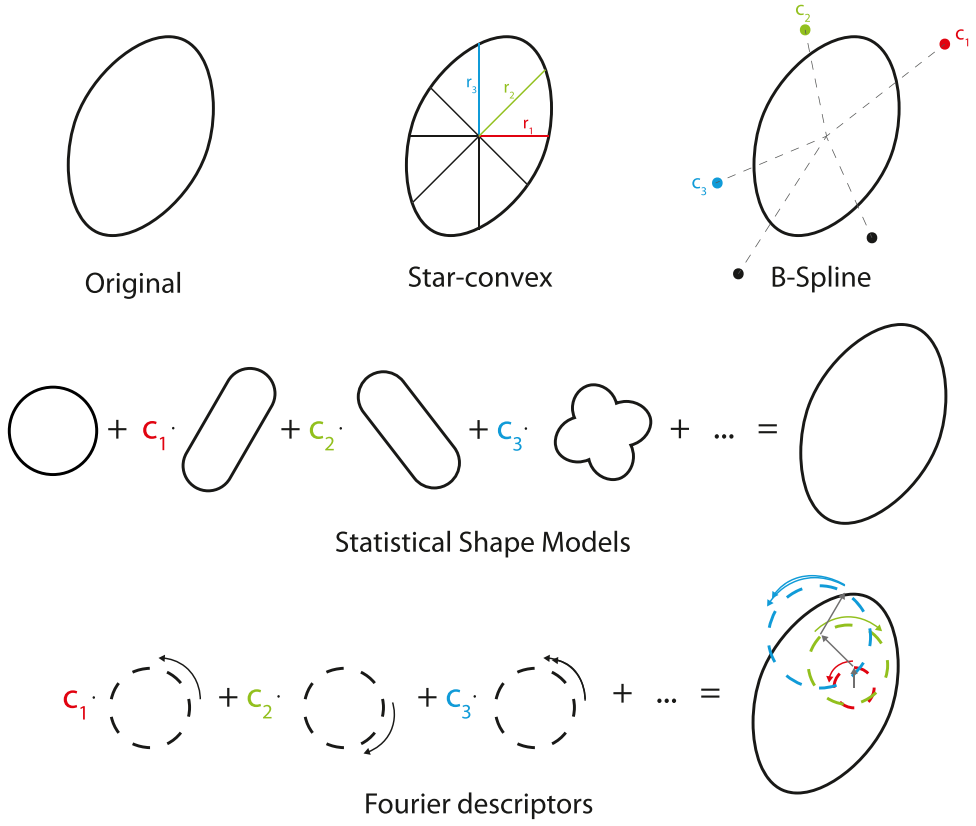

Fig. 1. Visual comparison of different cell representations. Star-convex polygons represent cells by the lengths of equiangular rays. The B-spline model implicitly defines the contour with the help of control points. Statistical shape models extract the most meaningful shape variations from a training dataset and def ines an unseen shape with the combination of the shape variations. The Fourier representation is defined by the sum of the modifications of unit circles rotating at certain frequencies.

experiment are star-convex polygons, B-splines, Fourier descriptors and statistical shape models. The first two representations have already seen use in CNN-s, thus, our aim is to incorporate the latter two into neural networks.

3.2. Cell segmentation

Our network takes an input image, and predicts the parameters of the underlying cell model describing the object at pixel (i, j), thus yielding a prediction map $\hat{C}_{ij} = \{\hat{c}_{ij}^n\}_{n=0}^N$. For the Fourier-based representation, we make one slight modification on one of the predicted coefficients: instead of predicting c_{ij}^0 explicitly (which is the center of mass of the predicted contour), we train our model to learn Δc_{ij}^0, which describes the translation of the center of mass of the object relative to pixel (i, j). For the SSM-based representation, we predict the weights of the principal variation vectors and a relative translation, rotation, and uniform scaling parameter. Besides that, we also predict a probability value p_{ij} for every pixel (i, j) so that pixels with low object probability can be ignored. This step is done for every representation type. Once a prediction has been made for every pixel, a non-maximum suppression (NMS) step ensures that overlapping candidates are filtered out. Similarly to StarDist and SplineDist, we use a standard U-Net backbone (architecture unaltered compared to [24]) with an additional feature extraction layer at the end and we regress the object probabilities and shape descriptors separately (see Fig. 2). We used the following hyperparameters and augmentation strategy for training the models: Adam optimizer with learning rate $\lambda = 3 \times 10^{-4}$, batch sizes of 4, 300 epochs, no batch normalization and no dropout. We split the data into train/test/validation sets by: 80%/10%/10%. For data augmentation, we used horizontal and vertical flips and standard color augmentation. The proposed architecture can be seen in Fig. 2. As for the training loss, we impose two different objective functions:

1. For the Fourier coefficients, we calculate the loss function in a different way compared to CPN: we formulate the loss in the frequency space besides a binary cross entropy loss:

$$\mathscr{L}_{Fourier}(p_{ij}, \hat{p}_{ij}, C_{ij}, \hat{C}_{ij}) = \mathscr{L}_{BCE}(p_{ij}, \hat{p}_{ij}) + \alpha_1 \mathscr{L}_{freq}(p_{ij}, C_{ij}, \hat{C}_{ij}), \quad (2)$$

where $\mathscr{L}_{freq}$ is expressed by

$$\mathscr{L}_{freq}(p_{ij}, C_{ij}, \hat{C}_{ij}) = p_{ij} \cdot \mathbb{1}_{p_{ij} > 0} \cdot \frac{1}{N} \sum_{n=0}^{N-1} |\mathbf{c}_{ij}^n - \hat{\mathbf{c}}_{ij}^n| + \alpha_2 \cdot \mathbb{1}_{p_{ij}=0} \cdot \frac{1}{N} \sum_{n=0}^{N-1} |\hat{\mathbf{c}}_{ij}^n|. \quad (3)$$

2. In case of the SSM-based representation, we formulate a loss function similar to SplineDist: the predicted parameters implicitly define a contour, and the loss function expresses the Euclidean distance between the ground truth and the predicted contours S_{ij} and $\hat{S}_{ij}$ respectively, with $\mathbf{s}_{ij}^n$ denoting the n-th contour coordinate). This has to be done because 'ground truth parameters' are not defined in this representation as opposed to the case of Fourier coefficients:

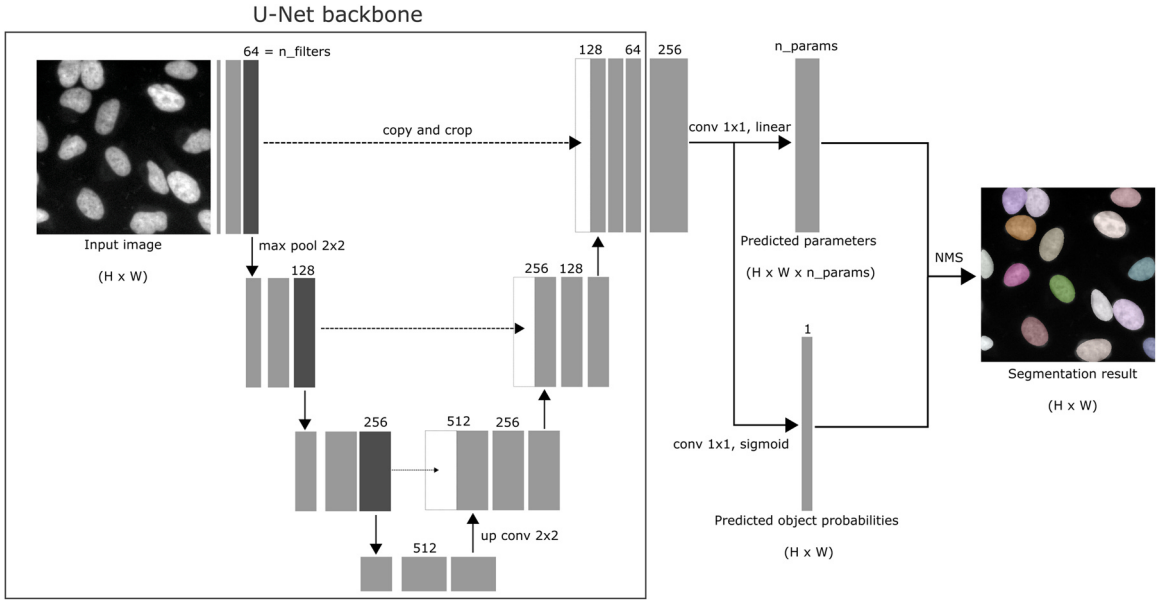

Fig. 2. Architecture of the proposed network.

$$\mathscr{L}_{SSM}(p_{ij}, \hat{p}_{ij}, S_{ij}, \hat{S}_{ij}) = \mathscr{L}_{BCE}(p_{ij}, \hat{p}_{ij}) + \alpha_1 \mathscr{L}_{contour}(p_{ij}, S_{ij}, \hat{S}_{ij}), \tag{4}$$

where $\mathscr{L}_{contour}$ is expressed by

$$\mathscr{L}_{contour}(p_{ij}, S_{ij}, \hat{S}_{ij}) = p_{ij} \cdot \mathbb{1}_{p_{ij} > 0} \cdot \frac{1}{N} \sum_{n=0}^{N-1} |\mathbf{s}_{ij}^n - \hat{\mathbf{s}}_{ij}^n| + \alpha_2 \cdot \mathbb{1}_{p_{ij}=0} \cdot \frac{1}{N} \sum_{n=0}^{N-1} |\hat{\mathbf{s}}_{ij}^n|. \tag{5}$$

4. Results and discussion

4.1. Datasets

To quantify the capabilities of the aforementioned representation techniques and segmentation methods, we used shapes and images from 5 different datasets.

1. **BBBC038v1**: A common benchmarking dataset for cell segmentation with star-convex shapes, available from the Broad Bioimage Benchmark Collection [1]. This dataset contains images from different modalities, but we only use the fluorescence microscopy ones (497 images) similarly to [24]. The images have varying resolutions, but we selected random crops of size 256×256 from them. The dataset contains ground truth annotations.
2. **BBBC021v1**: A dataset containing cytoplasm segmentations [2], available from the Broad Bioimage Benchmark Collection [16]. The original dataset contains 39,600 image files, but we only selected 5 of them, as this dataset was only used to evaluate the cell representation methods (no training required). The images were manually annotated by experts as there was no ground truth available in this set.
3. **The Cancer Genome Atlas (TCGA)**: A set of histopathology images containing 21,623 annotated nuclei from 7 different cancer types [14]. We used the same images as the ones used in [10]. The images have a resolution of 1000×1000, from which we selected random crops of size 256×256. The dataset contains ground truth annotations.
4. **KIMIA**: This dataset contains binary masks of various objects that are used in the field of shape analysis [25]. We selected 13 different shape classes from this set to evaluate the different cell representation methods. We used this dataset to evaluate the representation methods, thus closed contours were extracted from the binary masks to test the representation techniques.

4.2. Metrics

To evaluate the cell representation techniques, we used the common intersection over union (Jaccard index, or IoU) [12] metric:

$$IoU(x, y) = \frac{|x \cap y|}{|x \cup y|} = \frac{|x \cap y|}{|x| + |y| - |x \cap y|}. \tag{6}$$

For quantitative evaluation of the segmentation methods, we used the well adapted, official 2018 Data Science Bowl metric (DSB

Table 1
Shape representation scores averaged over all shapes on different datasets and parameter settings. Only the best performing representations with the highest scores (based on IoU) are shown. SSM: Statistical shape model, SC: Star-convex, BSpl: B-spline, FD: Fourier descriptors.

nparams	BBBC038v1	Synthetic	BBBC021v1	KIMIA
3	SSM (0.877)	BSpl (0.759)	SSM, BSpl (0.701)	SSM (0.624)
5	SSM (0.905)	BSpl (0.859)	BSpl (0.775)	FD (0.699)
7	SC (0.923)	FD (0.919)	FD (0.824)	FD (0.779)
9	SC (0.942)	FD (0.937)	FD, BSpl (0.86)	FD (0.824)
11	SC (0.95)	FD (0.942)	FD, BSpl (0.883)	FD, BSpl (0.847)
13	SC (0.956)	FD (0.946)	BSpl (0.902)	FD (0.874)
15	SC (0.958)	FD (0.947)	FD (0.912)	BSpl (0.887)
17	SC (0.963)	FD (0.948)	FD (0.921)	FD (0.908)
19	SC (0.965)	FD (0.948)	FD (0.928)	FD, BSpl (0.919)
21	SC (0.967)	FD (0.948)	FD (0.933)	FD (0.929)

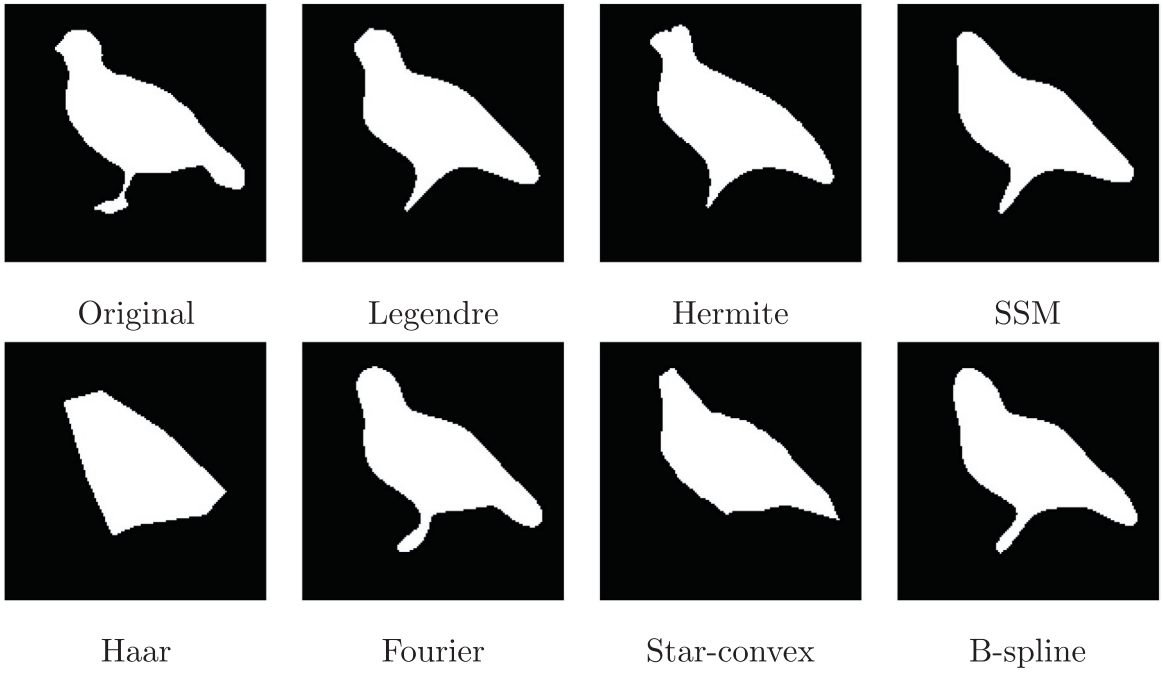

Fig. 3. Sample object from the KIMIA dataset and its reconstruction from 19 coefficients with different representations.

score, sometimes also referred to as "average precision") [1] averaged over different IoU threshold values:

$$Score = \frac{1}{|thresholds|} \sum_{\tau \in thresholds} S_\tau, \tag{7}$$

where

$$S_\tau = \frac{TP_\tau}{TP_\tau + FP_\tau + FN_\tau}, \tag{8}$$

and $thresholds = \{0.5, 0.55, \ldots, 0.85, 0.9\}$. The reason why we do not use IoU for evaluation similar to the representation evaluation is that for the representations, we need a pixel-wise score to quantify the best approaches (as we want to find the representation with the best approximation properties), whereas for instance segmentation tasks, object-wise metrics are used such as (7).

4.3. Evaluation of shape representations

To quantify the capabilities of the representations mentioned in Section 3.1, we evaluated them on randomly selected objects (masks) from the BBBC038v1 ($n\_objects = 285$), Synthetic ($n\_objects = 118$), BBBC021v1 ($n\_objects = 50$), KIMIA ($n\_objects = 26$) datasets. Each object was approximated individually with every representation technique, and the average IoU score was calculated for every dataset. We selected the best performing representation method(s) for increasing number of parameters (see Table 1) to see which ones work particularly well for certain datasets, or whether there are techniques that have an advantage at low or high number of parameters. According to our results (see Fig. 3 and Table 1), the star-convex representation performed the best on cell masks from the BBBC038v1 dataset, however, for other types of shapes, it did not yield competitive scores. This can mainly be attributed to the morphologies of the shapes, as the BBBC038v1 dataset mainly consists of regular, radially convex cell shapes, whereas other datasets have higher variation in terms of possible shapes. For the Synthetic, BBBC021v1, and KIMIA masks, the Fourier representation and B-splines yielded the highest IoU scores. Polynomial basis functions and Haar wavelets did not gain an edge in either of the datasets mentioned before. For polynomial basis functions, this can be attributed to the fact that these representations are not specifically designed to approximate closed contours, whereas Haar wavelets performed similarly to Fourier descriptors despite not yielding the best IoU scores any tested dataset. Statistical shape models performed the best when the number of parameters used for the representation were low, as this representation incorporates the most meaningful shape variations in the first few eigenvectors.

Table 2
Training time for the compared baseline methods. We measured the average time required to perform one step in an epoch.

	Fourier	StarDist	SplineDist	SSM	U-Net	Mask R-CNN
Training time (ms/step)	850 ms	850 ms	870 ms	1100 ms	**250 ms**	2600 ms

4.4. Evaluation of cell segmentation methods

To evaluate the efficiency of the different cell segmentation networks, we compared them on three different microscopic image datasets: the BBBC038v1, Synthetic, and TCGA. For reference, we use U-Net (2 class),[1] Mask R-CNN,[2] StarDist[3] and SplineDist[4] as baseline methods. We also measured the training time for every method, which can be seen in Table 2 (differences may be attributed to the different implementations of the algorithms). Our results indicate that if the objects to be segmented are star-convex, and the number of parameters for the cell model are high, then the star-convex polygon representation yields the highest scores. However, for only a few parameters, statistical shape models gave the best results on every dataset, which is expected, as the most meaningful principal variations should capture characteristic cell shape information.

[1] https://github.com/zhixuhao/unet.
[2] https://github.com/matterport/Mask_RCNN.
[3] https://github.com/stardist/stardist.
[4] https://github.com/uhlmanngroup/splinedist.

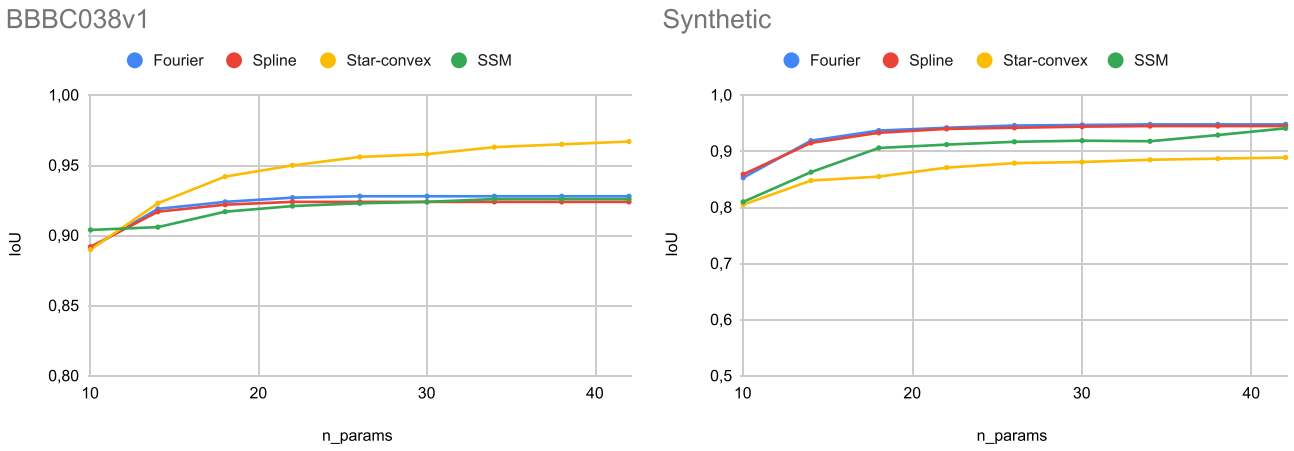

Fig. 4. Cell representation scores (average IoU) on the BBBC038v1 (left) and Synthetic (right) datasets. A performance plateau is observable for every cell model on both graphs.

When there are irregular, non star-convex shapes in the dataset (e.g. Synthetic), Fourier descriptors outperformed all of the other representations. This can be observed both quantitatively and qualitatively (Figs. 5, 6). As can be seen in Table 3, shape constrained methods were competitive with the baseline convoluational networks in every dataset. An interesting, yet counterintuitive result that we could observe was that by increasing the number of parameters for the cell models, the segmentation performance did not necessarily increase (see Fig. 6). A possible explanation for this could be that for some representations, more parameters mean just some additional minor variations to the shapes, which increase the complexity of the model but don't add substantial improvement to the representation itself (see Fig. 4), thus, they will just make the learning process harder Figs. 5, 6.

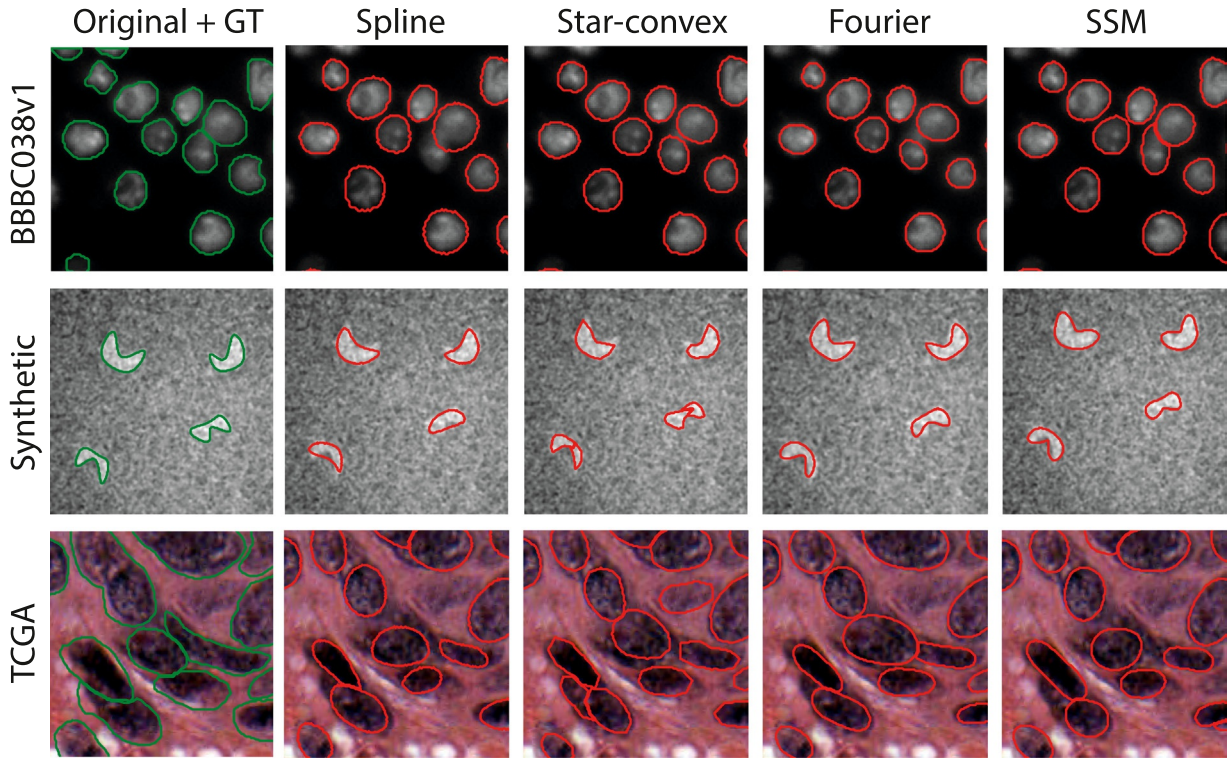

Fig. 5. Sample segmentation results on three different datasets with various shape model-based networks. For regular cell shapes, all representations yield acceptable results, however, for irregular objects (e.g. second row), the difference in performance is noticeable.

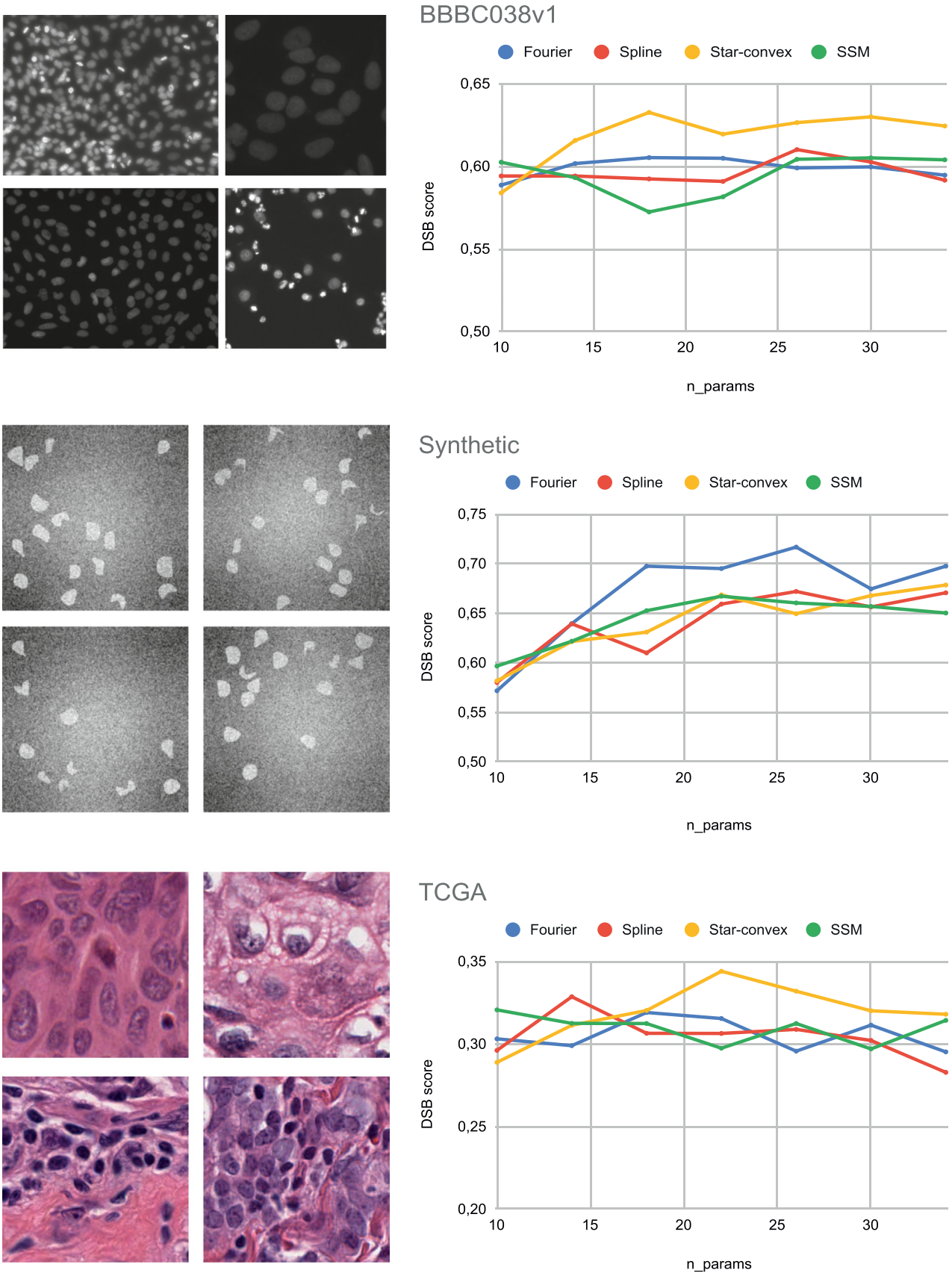

Fig. 6. Performance of the segmentation networks on three different datasets (sample images: left, scores: right). y-axis denotes the final DSB score.

Table 3
Cell detection results for 3 different datasets and *n_params* = 26 for the shape-constrained methods. Score denotes the official DSB score defined in (7) with additional metrics included for different IoU thresholds τ.

Model	Score	$S_{0.5}$	$S_{0.6}$	$S_{0.7}$	$S_{0.8}$	$S_{0.9}$
BBBC038v1						
Fourier	0.60	0.83	**0.79**	0.69	0.48	0.14
StarDist	**0.63**	**0.84**	**0.79**	**0.71**	**0.53**	0.19
SplineDist	0.61	**0.84**	0.78	0.70	0.49	0.12
SSM	0.60	0.83	0.78	0.70	0.50	0.13
U-Net	0.49	0.68	0.58	0.53	0.42	0.18
Mask R-CNN	0.59	0.83	0.76	0.69	0.48	**0.21**
Synthetic						
Fourier	**0.72**	**0.90**	0.86	**0.81**	**0.66**	0.30
StarDist	0.65	0.81	0.75	0.70	0.55	**0.40**
SplineDist	0.67	0.89	**0.87**	**0.81**	0.54	0.19
SSM	0.66	0.89	0.85	0.74	0.54	0.17
U-Net	0.67	0.83	0.74	0.73	0.56	0.38
Mask R-CNN	0.66	0.83	0.75	0.72	0.57	**0.40**
TCGA						
Fourier	0.30	0.60	0.48	0.30	0.10	0.00
StarDist	**0.33**	**0.61**	0.51	**0.37**	**0.15**	0.01
SplineDist	0.31	0.60	0.50	0.32	0.12	0.01
SSM	0.31	0.57	0.49	0.34	0.14	0.01
U-Net	0.23	0.48	0.41	0.22	0.01	0.00
Mask R-CNN	**0.33**	0.60	**0.52**	0.35	0.13	**0.02**

5. Conclusions

We reviewed and compared some of the most widely used shape representations from the literature and evaluated their efficiency on various datasets. Besides that, we also incorporated the most effective representations (besides the ones already available) into an end-to-end, U-net based CNN and tested them on three different microscopy datasets. We also compared our methods to other shape constrained cell segmentation models and well established baselines. Although shape representation-based methods are competitive alternatives to the most well adapted deep learning algorithms, their real strength can be observed on particular datasets: Star-convex polygons work very well for regular, radially convex objects. Fourier descriptors are especially useful if there are irregular, non star-convex shapes in the dataset, whereas statistical shape models perform best when the number of cell model parameters are low. Finding optimal basis shapes suited for certain cell types could be an interesting continuation of this research, as well as studying the different optimal representations for various segmentation tasks. Further research could also focus on the exploration of how the weights of the pre-defined cell models can be effectively learned by neural networks.

CRediT authorship contribution statement

Dominik Hirling: Conceptualization, Data curation, Formal analysis, Investigation, Methodology, Software, Validation, Visualization, Writing – original draft, Writing – review & editing. **Peter Horvath:** Conceptualization, Formal analysis, Funding acquisition, Investigation, Methodology, Project administration, Resources, Supervision, Writing – original draft, Writing – review & editing.

Conflicts of interest statement

The authors declare no conflicts of interest.

Acknowledgements

This work was supported by the LENDULET-BIOMAG Grant (2018–342), the H2020 (ERAPERMED-COMPASS, FAIR-CHARM), the OTKA-SNN 139455 and the Chan Zuckerberg Initiative (Deep Visual Proteomics). Prepared with the professional support of the Doctoral Student Scholarship Program of the Co-operative Doctoral Program of the Ministry of Innovation and Technology financed from the National Research, Development and Innovation Fund.

References

[1] Caicedo Juan C, Goodman Allen, Karhohs Kyle W, Cimini Beth A, Ackerman Jeanelle, Haghighi Marzieh, et al. Nucleus segmentation across imaging experiments: the 2018 data science bowl. Nat Methods 2019;16(12):1247–53.
[2] Caie Peter D, Walls Rebecca E, Ingleston-Orme Alexandra, Daya Sandeep, Houslay Tom, Eagle Rob, et al. High-content phenotypic profiling of drug response signatures across distinct cancer cellsphenotypic profiling across cancer cell types. Mol Cancer Therap 2010;9(6):1913–26.
[3] Chiao Jui-Ying, Chen Kuan-Yung, Liao KenYing-Kai, Hsieh Po-Hsin, Zhang Geoffrey, Huang Tzung-Chi. Detection and classification the breast tumors using mask r-cnn on sonograms. Medicine 2019;98(19).
[4] Cootes Timothy F, Taylor Christopher J, Cooper David H, Graham Jim. Active shape models-their training and application. Comput Vision Image Understand 1995;61(1):38–59.
[5] Eschweiler Dennis, Rethwisch Malte, Koppers Simon, Stegmaier Johannes. Spherical harmonics for shape-constrained 3d cell segmentation. In: 2021 IEEE 18th international symposium on biomedical imaging (ISBI), IEEE; 2021. p. 792–6..
[6] Donahue Jeff, Darrell Trevor, Malik Jitendra, Girshick Ross, Rich feature hierarchies for accurate object detection and semantic segmentation. In Proceedings of the IEEE conference on computer vision and pattern recognition; 2014. p. 580–7.
[7] Gower John C. Generalized procrustes analysis. Psychometrika 1975;40(1):33–51.
[8] He Kaiming, Gkioxari Georgia, Dollár Piotr, Girshick Ross, Mask r-cnn. In Proceedings of the IEEE international conference on computer vision; 2017. p. 2961–9.
[9] He Kaiming, Zhang Xiangyu, Ren Shaoqing, Sun Jian. Deep residual learning for image recognition.In Proceedings of the IEEE conference on computer vision and pattern recognition; 2016. p. 770–8.
[10] Hollandi Reka, Szkalisity Abel, Toth Timea, Tasnadi Ervin, Molnar Csaba, Mathe Botond, et al. nucleaizer: a parameter-free deep learning framework for nucleus segmentation using image style transfer. Cell Syst 2020;10(5):453–8.
[11] Isensee Fabian, Jaeger Paul F, Kohl Simon AA, Petersen Jens, Maier-Hein Klaus H. nnu-net: a self-configuring method for deep learning-based biomedical image segmentation. Nat methods 2021;18(2):203–11.
[12] Jaccard Paul. Étude comparative de la distribution florale dans une portion des alpes et des jura. Bull Soc Vaudoise Sci Nat 1901;37:547–79.
[13] Jetley Saumya, Sapienza Michael, Golodetz Stuart, Torr Philip H.S.Straight to shapes: real-time detection of encoded shapes. In Proceedings of the IEEE conference on Computer Vision and Pattern Recognition; 2017. p. 6550–9.
[14] Kumar Neeraj, Verma Ruchika, Sharma Sanuj, Bhargava Surabhi, Vahadane Abhishek, Sethi Amit. A dataset and a technique for generalized nuclear

segmentation for computational pathology. IEEE Trans Med Imaging 2017;36(7):1550–60.
[15] Lin Tsung-Yi, Dollár Piotr, Girshick Ross, He Kaiming, Hariharan Bharath, Belongie Serge. Feature pyramid networks for object detection. In: Proceedings of the IEEE conference on computer vision and pattern recognition; 2017 p. 2117–25.
[16] Ljosa Vebjorn, Sokolnicki Katherine L, Carpenter Anne E. Annotated high-throughput microscopy image sets for validation. Nat methods 2012;9(7). 637-637.
[17] Long Feixiao. Microscopy cell nuclei segmentation with enhanced u-net. BMC Bioinform 2020;21(1):1–12.
[18] Mandal Soham, Uhlmann Virginie. Splinedist: Automated cell segmentation with spline curves. In 2021 IEEE 18th international symposium on biomedical imaging (ISBI). IEEE; 2021. p. 1082–6.
[19] Marcos, Diego, Tuia Devis, Kellenberger Benjamin, Zhang Lisa, Bai Min, Liao Renjie, Urtasun Raquel. Learning deep structured active contours end-to-end. In: Proceedings of the IEEE conference on computer vision and pattern recognition; 2018. p. 8877–85.
[20] Miksys Laurynas, Jetley Saumya, Sapienza Michael, Golodetz Stuart, Torr Philip H.S. Straight to shapes++: real-time instance segmentation made more accurate. arXiv preprint arXiv:1905.11358; 2019.
[21] Oktay Ozan, Schlemper Jo, Le Folgco Loic, Lee Matthew, Heinrich Mattias, Misawa Kazunari et al. Attention u-net: Learning where to look for the pancreas. arXiv preprint arXiv:1804.03999; 2018.
[22] Pincus Zachary, Theriot JA. Comparison of quantitative methods for cell-shape analysis. J Microscopy 2007;227(2):140–56.
[23] Ronneberger Olaf, Fischer Philipp, Brox Thomas. U-net: Convolutional networks for biomedical image segmentation. In: Proceedings of international conference on medical image computing and computer-assisted intervention. Springer; 2015. p. 234–41.
[24] Schmidt Uwe, Weigert Martin, Broaddus Coleman, Myers Gene. Cell detection with star-convex polygons. In: Proceedings of international conference on medical image computing and computer-assisted intervention. Springer; 2018. p. 265–73.
[25] Sharvit Daniel, Chan Jacky, Tek Hüseyin, Kimia Benjamin B. Symmetry-based indexing of image databases. J Visual Commun Image Represent 1998;9(4):366–80.
[26] Upschulte Eric, Harmeling Stefan, Amunts Katrin, Dickscheid Timo. Contour proposal networks for biomedical instance segmentation. Med Image Anal 2022:102371.
[27] Weigert Martin, Schmidt Uwe, Haase Robert, Sugawara Ko, Myers Gene. Star-convex polyhedra for 3d object detection and segmentation in microscopy. In: Proceedings of the IEEE/CVF winter conference on applications of computer vision; 2020. p. 3666–73.
[28] Wu Pei-Hsun, Phillip Jude M, Khatau Shyam B, Chen Wei-Chiang, Stirman Jeffrey, Rosseel Sophie, et al. Evolution of cellular morpho-phenotypes in cancer metastasis. Sci Rep 2015;5(1):1–10.
[29] Zahn Charles T, Roskies Ralph Z. Fourier descriptors for plane closed curves. IEEE Trans Comput 1972;100(3):269–81.